

# Optical binding via surface plasmon polariton interference

Natalia Kostina<sup>1</sup>, Aliaksandra Ivinskaya<sup>1</sup>, Sergey Sukhov<sup>2</sup>, Andrey Bogdanov<sup>1</sup>, Ivan Toftul<sup>1,3</sup>,  
Manuel Nieto-Vesperinas<sup>4</sup>, Pavel Ginzburg<sup>1,5</sup>, Mihail Petrov<sup>1,3</sup>, and Alexander Shalin<sup>1</sup>

<sup>1</sup>*ITMO University, Department of Nanophotonics and Metamaterials, Saint-Petersburg, 199034, Russia*

<sup>2</sup>*CREOL, University of Central Florida, Tampa, 32816-2700, USA*

<sup>3</sup>*Saint-Petersburg Academic University, Saint-Petersburg, 194021, Russia*

<sup>4</sup>*Instituto de Ciencia de Materiales de Madrid, Consejo Superior de Investigaciones Cientificas,  
Campus de Cantoblanco, Madrid E-28049, Spain and*

<sup>5</sup>*School of Electrical Engineering, Tel Aviv University, Tel Aviv, 6997801, Israel*

(Dated: January 22, 2018)

Optical binding allows creation of mechanically stable nanoparticle configurations owing to formation of self-consistent optical trapping potentials. While the classical diffraction limit prevents achieving deeply subwavelength arrangements, auxiliary nanostructures enable tailoring optical forces via additional interaction channels. Here, a dimer configuration next to metal surface was analyzed in details and the contribution of surface plasmon polariton waves was found to govern the interaction dynamics. It was shown that the interaction channel, mediated by resonant surface waves, enables achieving subwavelength stable dimers. Furthermore, the vectorial structure of surface modes allows binding between two dipole nanoparticles along the direction of their dipole moments, contrary to vacuum binding, where a stable configuration is formed in the direction oriented perpendicularly to the polarization of dipole moments. In addition, the enhancement of optical binding stiffness for one order of magnitude was predicted owing to the surface plasmon polariton interaction channel. These phenomena pave a way for developing new flexible optical manipulators, allowing for the control over a nanoparticle trajectory on subwavelength scales and opens a room of opportunities for optical-induced anisotropic, i.e. with different periods along the field polarization as well as perpendicular to it, organization of particles on a plasmonic substrate.

## INTRODUCTION

Light carries momentum which can influence matter through optical forces enabling manipulation of micro and nanoscale objects<sup>1</sup> and even atom ensembles<sup>2</sup>. The methods of optical tweezing<sup>3,4</sup> rely on attraction of small objects to the regions of high field intensity. Spatially non-uniform intensity distributions used for positioning microobjects at predefined pattern can be achieved with a nanostructured environment or by interference of several beams. Yet, since early years of optical tweezing experiments, it was discovered that several particles tend to self-organize under homogeneous illumination<sup>5,6</sup>. This effect is referred to as transverse optical binding. The interference between incident and scattered light, owing to interaction with particles, results in the formation of a set of potential wells defining stable positions of particles. Optical binding has been intensively studied both theoretically<sup>7-11</sup> and experimentally<sup>12-16</sup> also as a prospective method for self-organization of particles. However, the strength of optical binding drops rapidly with nanoparticle size as the scattering efficiency decreases as  $\sim R^6$ , where  $R$  is the nanoparticle radius. On the other hand, the viscous damping is also reduced for smaller particles, which makes the fluctuations and stochastic processes in liquids to be more influential. As a result, for reliable optical control of subwavelength nanoparticles, strong optical fields are required. In order to achieve this without strong heating of the surrounding media, it was suggested to use plasmonic structures, which can enhance optical fields locally. The opti-

cal binding can be enhanced by localized plasmon resonance in the nanoparticles<sup>8,17,18</sup>. The localized plasmons can improve trapping efficiency at hot spots of corrugated metal<sup>19,20</sup>, or provide particle acceleration against beam direction in plasmonic V-grooves<sup>21</sup>. Three dimensional structures of plasmonic particles, such as metamaterials, can be also employed to trap or manipulate nanoparticles, e.g., for realization of optical pulling forces attracting nanoparticles to a light source<sup>22,23</sup>. In the context of optical binding flat metal surfaces also may be very relevant. The excitation of propagating surface plasmon polaritons (SPPs) and induced optical thermal forces are responsible for self-organization of micron size nanoparticles<sup>24</sup>. Moreover, the direct momentum transfer from SPP to micron size particles<sup>25,26</sup> can be used for enhancing the optical forces near planar metallic surface, which can be used for sorting and ordering of nanoparticles<sup>15,27,28</sup>. Recently, it was suggested that SPP modes can open a way for manipulating the optical forces acting on nanosize particles by the directional excitation of the propagating SPP modes<sup>29-31</sup>.

Here, we propose a new mechanism of transverse optical binding via excitation of SPP modes (*SPP binding*) near a metallic planar interface. This mechanism is based on far-field interaction through the interference of SPP waves and is different to formation of resonant nanoparticle molecules due to their near field interaction<sup>17,18,32,33</sup>. Comparing to common transverse binding in a free space (*photon binding*), the proposed approach has several advantages: i) it can enhance the binding effect for small nanoparticles due to resonant excitation of SPP modes; ii) the distance between the bounded nanoparticles is de-

finer by the SPP effective wavelength and, thus, can be significantly smaller surpassing the diffraction limit; iii) the binding occurs in the direction of dipole polarization in accordance with the directivity of SPP emission, which differs from the case of a free space binding, where stable configurations are formed in the direction perpendicular to the dipole moments. In this paper, we theoretically show how SPP-based transverse optical binding can bring new features to nanoparticle trapping and manipulation.

## I. NANOPARTICLES POLARIZATION NEAR A SUBSTRATE

We consider two identical nanoparticles placed close to a planar metallic interface at coordinates  $\mathbf{r}_1$ , and  $\mathbf{r}_2$  in the field of a normally incident plane wave (see Fig. 1). We assume that nanoparticles have radius  $R$  and are made of dielectric material with permittivity  $\epsilon$ . In the dipole approximation the radius of nanoparticles  $R$  is much smaller than the typical scale of electric field variations. In this limit, the optical force acting on a nanoparticle is given by the expression<sup>34</sup>

$$\mathbf{F} = \frac{1}{2} \text{Re} \sum_i p_i^* \nabla E_i(\mathbf{r}, \omega), \quad (1)$$

where  $E_i(\mathbf{r}, \omega)$  is the  $i$ -th component of a local field.

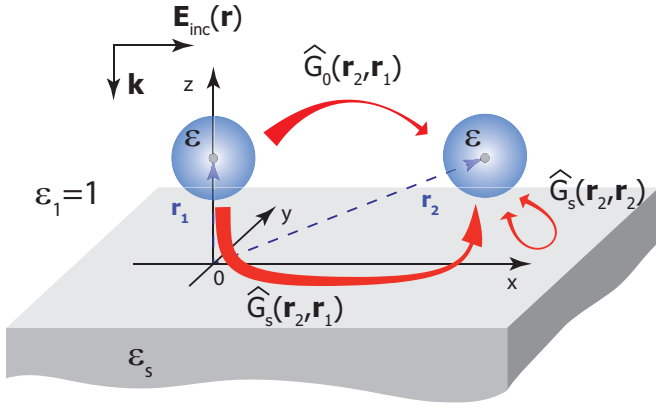


FIG. 1. The scheme of the problem. Nanoparticles with permittivity  $\epsilon$  are positioned at equal distances from a surface  $z_1 = z_2 = z$ . We assume that the permittivity of the upper half-space equals to  $\epsilon_1 = 1$ .

The dipole moment of a nanoparticle  $\mathbf{p}(\mathbf{r})$  is defined as  $\mathbf{p}(\mathbf{r}) = \alpha(\omega)\mathbf{E}(\mathbf{r})$ , where  $\alpha(\omega)$  is the vacuum dipole polarizability corrected with account for retardation effects:

$$\frac{1}{\alpha} = \frac{1}{\alpha_0} - \frac{ik_0^3}{6\pi\epsilon_0}, \quad \alpha_0 = 4\pi\epsilon_0 R^3 \frac{\epsilon - \epsilon_1}{\epsilon + 2\epsilon_1}, \quad (2)$$

where  $k_0$  is the wavevector in a free space, and  $\epsilon_0$  is the vacuum permittivity. The local electric field includes the incident plane wave, multiply rescattered field between

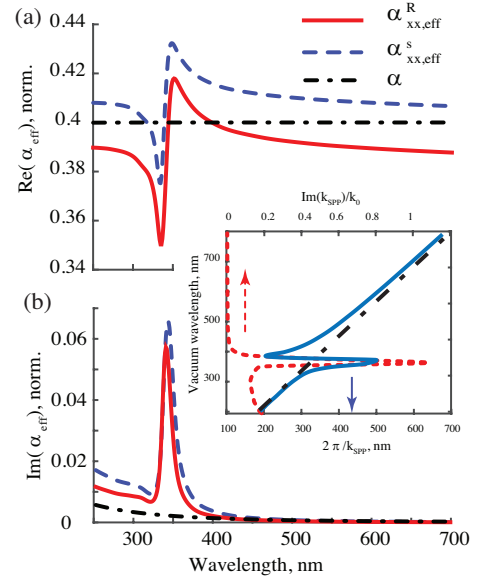


FIG. 2. The spectrum of real (a) and imaginary (b) parts of the  $xx$ -components of effective polarizability tensor  $\hat{\alpha}_{eff}^s$  (blue dashed line) and  $\hat{\alpha}_{eff}^R$  (red solid line) shown along with vacuum polarizability  $\alpha$  (black dash-dot line). The polarizability is normalized over  $4\pi\epsilon_0 R^3$ , and calculated for a nanoparticle of radius  $R = 15$  nm with  $\epsilon = 3$  whose center is located above the surface at  $z = 20$  nm. The inset shows the dependence of the SPP typical period denoted as  $L_{SPP} = 2\pi/k_{SPP}$  (upper  $x$ -axis), and imaginary part of SPP wavevector (lower  $x$ -axis) on the vacuum wavelength.

particles via free-space and substrate channels, and self-induced contribution of each particle through the reflection from the substrate. The local field is given by

$$\mathbf{E}(\mathbf{r}) = \mathbf{E}_0(\mathbf{r}) + \frac{k_0^2}{\epsilon_0} \hat{G}(\mathbf{r}, \mathbf{r}_1) \mathbf{p}_1 + \frac{k_0^2}{\epsilon_0} \hat{G}(\mathbf{r}, \mathbf{r}_2) \mathbf{p}_2. \quad (3)$$

Here, the first term in the right hand side is the amplitude of the external field, the second and third terms correspond to the field generated by the first and second nanoparticles respectively. The total Green's function  $\hat{G}(\mathbf{r}, \mathbf{r}_0) = \hat{G}_0(\mathbf{r}, \mathbf{r}_0) + \hat{G}_s(\mathbf{r}, \mathbf{r}_0)$  is a sum of the scattered  $\hat{G}_s$  and vacuum  $\hat{G}_0$  components respectively<sup>35</sup>. One can simplify the consideration if renormalizes the polarizability tensor with respect to the self-action Green's function component  $\hat{G}_s(\mathbf{r}_i, \mathbf{r}_i)$  term.

$$\mathbf{p}_i = \hat{\alpha}_{i,eff}^s \left( \mathbf{E}_0(\mathbf{r}_i) + \frac{k_0^2}{\epsilon_0} \hat{G}(\mathbf{r}_i, \mathbf{r}_j) \mathbf{p}_j \right), \quad (4)$$

$$i = 1, 2 \quad j = 2, 1.$$

Here, we have introduced the effective polarizability tensor  $\hat{\alpha}_{i,eff}^s$  as follows:

$$\hat{\alpha}_{i,eff}^s(\mathbf{r}_i, \omega) = \alpha(\omega) \left( 1 - \alpha(\omega) \frac{k_0^2}{\epsilon_0} \hat{G}_s(\mathbf{r}_i, \mathbf{r}_i, \omega) \right)^{-1}, \quad i=1,2. \quad (5)$$

This tensor gives a correction of a vacuum polarizability  $\alpha(\omega)$  with accounting for nanoparticle self-action through the substrate. This tensor is diagonal as  $\widehat{G}_s(\mathbf{r}_i, \mathbf{r}_i)$  is diagonal in the case of a flat isotropic substrate<sup>35</sup>.

For the sake of simplicity, in the following we fix the position of the first particle in the origin of the coordinate system at  $x_1 = 0$  and  $y_1 = 0$ , and will consider the force acting on the second particle only. Computing the field at the point of the dipole according to the expression in Eq. (3), one can achieve a system of equations for dipole moments  $\mathbf{p}_1$  and  $\mathbf{p}_2$  (see Appendix A), and, in the special case of normal incidence of the plane wave, the expression for the dipole moments can be simplified even further:

$$\mathbf{p}_i = \widehat{\alpha}_{i,eff}^R \mathbf{E}_0(\mathbf{r}_i), \quad (6)$$

$$\widehat{\alpha}_{i,eff}^R(\mathbf{r}_i, \omega) = \alpha(\omega) \left( 1 - \alpha(\omega) \frac{k^2}{\varepsilon_0} \widehat{G}_s(\mathbf{r}_i, \mathbf{r}_i, \omega) - \frac{k^4}{\varepsilon_0^2} \alpha(\omega) \widehat{G}(\mathbf{r}_i, \mathbf{r}_j) \widehat{\alpha}_{j,eff}^s(\mathbf{r}_j, \omega) \widehat{G}(\mathbf{r}_j, \mathbf{r}_i) \right)^{-1} \times \quad (7)$$

$$\left( 1 + \frac{k^2}{\varepsilon_0} \widehat{G}(\mathbf{r}_i, \mathbf{r}_j) \widehat{\alpha}_{j,eff}^s(\mathbf{r}_j, \omega) \right),$$

$$i = 1, 2 \quad j = 2, 1.$$

Now, the polarizability  $\widehat{\alpha}_{eff}^R$  (see the Appendix A for the details) includes all the interaction channels: (i) the self-action of nanoparticle through the substrate, and (ii) the cross-action of two nanoparticle via vacuum and substrate. Moreover, it is worth mentioning that though the effective polarizability tensor  $\widehat{\alpha}_{eff}^s$  is diagonal, the tensor  $\widehat{\alpha}_{eff}^R$  is non-diagonal as the presence of the second nanoparticle does not preserve translational symmetry of the system.

The excitation of SPP modes affects both the effective polarizability due to the substrate mediated self-action, and cross action of nanoparticles. The spectra of real and imaginary parts of  $xx$  - components of  $\widehat{\alpha}_{eff}^R$  (solid line) and  $\widehat{\alpha}_{eff}^s$  (dashed line) are plotted in Fig. 2 for the case of silver substrate. The vacuum polarizability  $\alpha$  is also shown in the figure with dash-dot line. One can see that the effective polarisabilities have resonance at around 350 nm. From the inset of Fig. 2, one can see that this wavelength corresponds to SPP resonant excitation for silver/vacuum interface, which is defined by the condition  $\text{Re}(\varepsilon_s(\omega)) + 1 = 0$  and also corresponds to maximal value of real part of SPP wavevector  $k_{SPP} = k_0 \sqrt{\varepsilon_s / (\varepsilon_s + 1)}$ . In the inset the effective wavelength of SPP mode defined as  $L_{SPP} = 2\pi / k_{SPP}$  is also shown. The strong enhancement of the imaginary part of the effective polarizability is a sign of strong rescattering of light into the SPP mode.

## II. DETERMINING THE STABLE CONFIGURATIONS

By determining the dipole moments of nanoparticles, one can calculate the optical force acting on each

nanoparticle using the expression (1) (see the details in the Appendix Eq. (A13)). In the following, we will refer to the optical force acting on the second nanoparticle only, fixing the first nanoparticle in the coordinate origin. In order to find the equilibrium positions of nanoparticle, we plot the dependence of the  $x$ -component of the optical force as a function of interparticle distance along  $x$ -axis as shown in Fig. 3 a). The force is normalized over the optical pressure force acting on the same nanoparticle in vacuum  $F_0 = 1/2k|E_0|^2\text{Im}(\alpha(\omega))$ , where  $|E_0|$  is the amplitude of the incident plane wave. One can see that the force changes at particular point on the  $x$ -axis denoting the equilibrium positions points. These points can be stable along  $x$  if the force is restoring (shown with solid circles, i.e. point 1), and unstable otherwise (shown with white filled circles). One should also note that when nanoparticles are close to each other the force goes to minus infinity, until the nanoparticles touch each other. However this case is out of the scope of the present paper.

To identify the role of plasmons in the interaction force we have excluded SPP contribution from the Green's function by integrating over the free space modes only in the spectral representation (see Appendix B). One can see that in the absence of SPPs the interaction force becomes one order of magnitude weaker, and the period between stable positions is significantly enlarged being defined by the vacuum wavelength and photons interference. Moreover, the equilibrium points shown with blue circles are stable both along  $x$  and  $y$  directions making them globally stable, which does not happen in case of photon binding. To illustrate this, we plotted the  $F_y$  force (see Fig. 3 b)) as function of the transverse angle  $\phi$  (see the inset in Fig. 3) in the vicinity of points of stable equilibrium positions. In Fig. 3 (c) one can see the dependence of the binding length on the vacuum wavelength shown along with the period of SPP wave, which is equal to  $L_{SPP}$ . One can see that the binding distance is fully defined by the period of the SPP wave when the excitation condition is fulfilled, thus, providing the binding at distances significantly shorter than vacuum wavelength. This also strongly differs from work of Salary et. al.<sup>17</sup>, where the optical forces between two nanoparticles over metallic substrate were considered in the regime, when the interaction force is mainly defined by the near-field components.

In order to support the results discussed above, we have performed numerical simulations in COMSOL Multiphysics package (see Fig. 3 (d), scatter line) and showed good correspondence with the obtained solution based on Green's function approach (see Fig. 3 (d) solid line). The Green's function approach shows good agreement with numerical results also at the distances comparable to nanoparticle size. Moreover, basing on Green's function formalism we have derived the approximate expression for the contribution of SPP mode into the optical force (see Appendix C for the details):

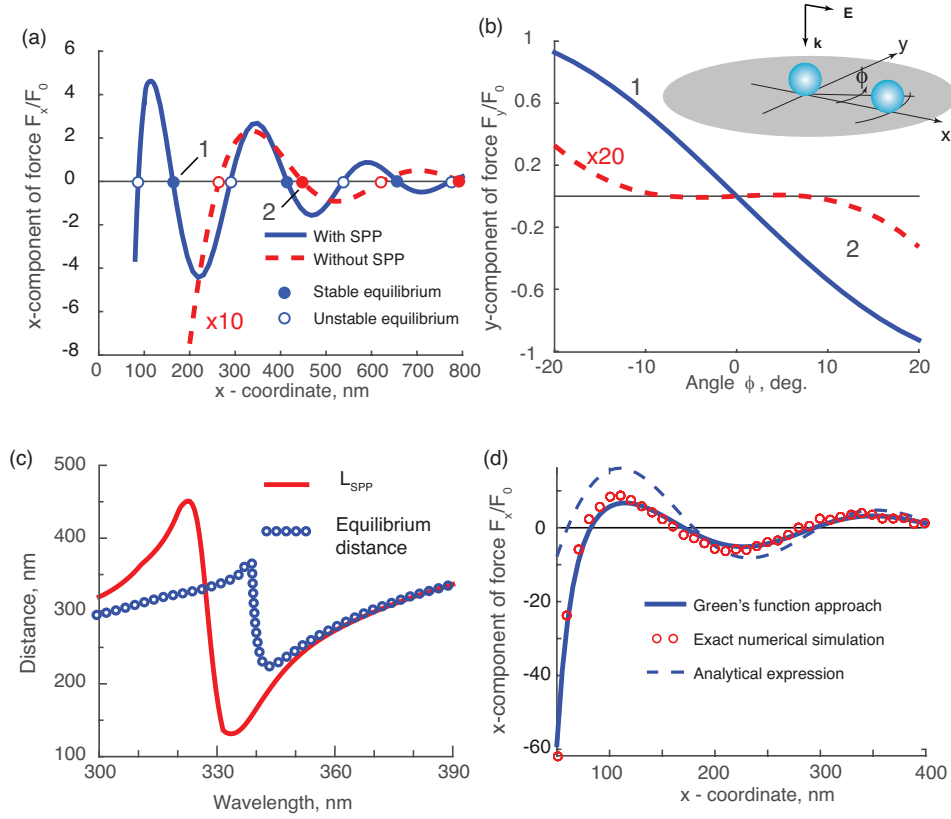


FIG. 3. (a) The  $x$ -component of optical force plotted along the  $x$ -axis coinciding with the direction of electric field polarization. The blue solid line denotes the force with account for all interaction channels. The red dashed line is for the interaction through the free space photons only. (b) The  $y$ -component of optical force in the direction transverse to the  $x$ -axis, showing the stability of the binding position in the direction perpendicular to the  $x$ -axis. The blue solid line and red dashed line correspond to force calculated with or without account for SPP interaction channel for the equilibrium positions labeled 1 and 2 in (a) correspondingly. The results are shown for the wavelength  $\lambda = 350$  nm. (c) The distance between the stable equilibrium positions obtained from (a) compared with the distance  $L = 2\pi/k_{SPP}$ . (d) The comparison of the optical force calculated within Green's function approach (same as in Fig.3 (a)) and calculated numerically with COMSOL Multiphysics package. The approximate analytical expression given by the Eq. (8) for SPP induced force is also shown with dashed line. All the results shown in the figure are computed for  $R = 15$  nm and  $z = 25$  nm.

$$F_x \approx \pi |p_x|^2 \text{Re} \left[ \frac{k_{SPP}^3 k_{1z}^2 k_{2z}}{k_0^2 (1 - \epsilon_s)} \times H_1^{(1)}(k_{SPP} x) \exp(-\text{Im}(k_{1z}) z) \right]. \quad (8)$$

Here  $k_{1z} = \sqrt{k_0^2 - k_{SPP}^2}$ , and  $k_{2z} = \sqrt{\epsilon_s k_0^2 - k_{SPP}^2}$  are  $z$ -components of SPP wavevector in the upper half-space and in the substrate correspondingly,  $H_1^{(1)}(q)$  is the first order Hankel function of the first kind. The derived expression very illustratively shows the origin of the SPP mode: the Hankel function describes the SPP mode excited by a dipole and propagating over a flat surface. Its zeros define the equilibrium positions of the nanoparticle. The  $z$ -components of the wavevector is complex since SPP is a localized wave, thus, the exponent in Eq. (8) shows that strength of dipole-SPP coupling decays.

One needs to stress, that the transverse binding in vacuum does not provide stable equilibrium positions

along  $x$ -axis<sup>36</sup>. This difference of SPP and photon binding can be understood through the difference in the scattering diagrams of SPPs and photons. This is illustrated in Fig.4 where two-dimensional maps of  $x$  and  $y$  force components are plotted. The photon binding is well-known to have stable configuration perpendicular to the field polarization direction in accordance with the dipole emission pattern (see Fig. 4 (a, b)). The SPP binding, on the contrary, has stable configurations along the polarization direction, in which preferable excitation of SPP modes occurs (see Fig. 4 (c, d)). It is also worth noting that the amplitudes of lateral forces are several times higher when SPP modes affect binding.

We illustrate the character of SPP binding by calculating the dynamics of the second nanoparticle motion in the force field of the first nanoparticle, which is fixed at the origin of the coordinates. We consider only two-dimensional motion of the nanoparticle, keeping the  $z$ -coordinate to be constant. The dynamics is obtained

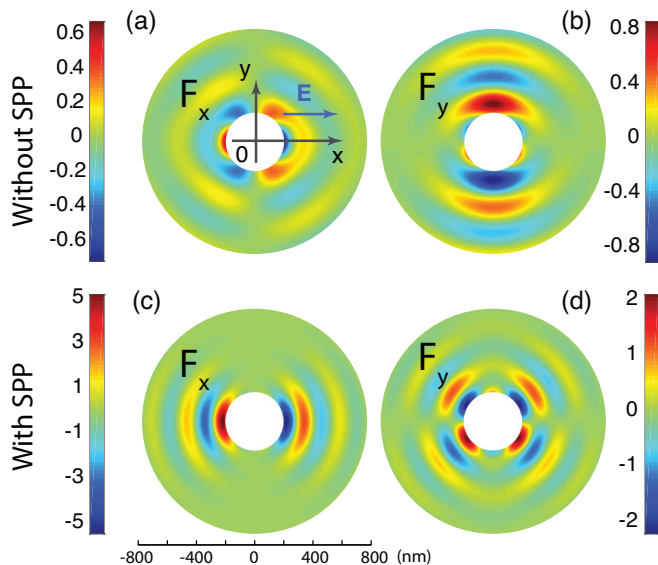


FIG. 4. The two-dimensional maps showing the  $x$  and  $y$  forces for SPP and photon binding. The different directionality of the scattering pattern is responsible for different geometry of stable equilibrium positions. The results are shown for wavelength  $\lambda = 350$  nm and  $z = 25$  nm.

through direct solution of equations of motion under the external optical force with the account for viscous damping. The details are discussed in Appendix D. Two typical trajectories are shown in Fig. 5 for two different sets of initial coordinates of the second nanoparticle. The color map shows the intensity of nanoparticle attraction to the equilibrium positions along  $x$ -axis. The arrows show the force field, while the lines show the trajectories with color changing from blue to red while time elapses. One can see that the nanoparticle actively tends to set the position along the  $x$ -axis where the binding force is the strongest.

The important parameter, which characterizes the stability of the equilibrium states, is the stiffness of the trap. At the equilibrium positions the total optical force is zero, but when shifted from the stable positions the nanoparticles undergo action of a restoring force, which is locally proportional to the amplitude of the displacement  $F_r = -\kappa_x \Delta x$ , with the parameter  $\kappa_x$  characterizing the stiffness of the system along the  $x$ -direction. However, this approximation of the restoring force only applies to the gradient component of the optical force. Indeed, we consider the nanoparticles significantly smaller than the wavelength, that results in low and non-resonant at the wavelengths imaginary part of the polarizability  $\text{Im}(\alpha_{eff}) \ll \text{Re}(\alpha_{eff})$ , as  $\text{Im}(\alpha_{eff}) \simeq (R^6/\lambda^3)$ , and  $R \ll \lambda$  (see Fig. 2). Thus, the radiation force, which is proportional to imaginary part of the polarizability, can be neglected (see Appendix E). The stiffness in the considered system strongly depends on the mechanism of the nanoparticles interaction, and, as can be seen from Fig. 3, it is much higher when the plasmon interaction

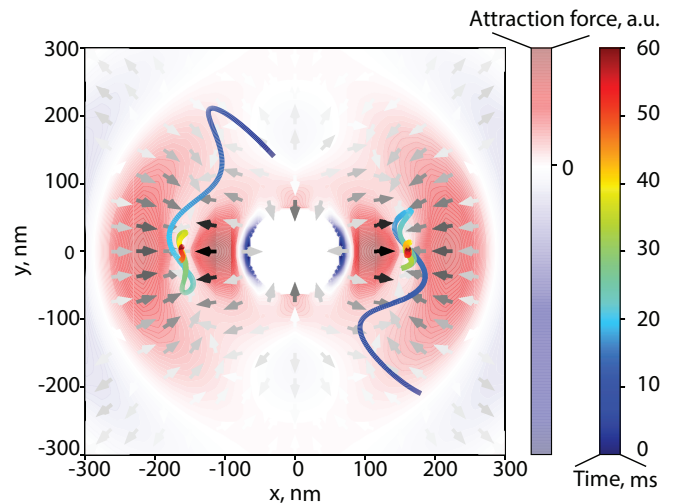


FIG. 5. The dynamics of the second nanoparticle motion. The first nanoparticle is fixed at the origin. The colour of the trajectory line denotes the time elapsed since the beginning of motion. The arrows show the force field: the darker are the arrows the stronger is the optical force. The colour map at the background shows the force which attracts or repulses nanoparticle to/from the equilibrium positions at  $y = 0$  and  $x = \pm 175$  nm. The intensity of the red colour gives the strength of nanoparticle attraction, while blue shows repulsion of the nanoparticle. The parameters of computation are  $R = 15$  nm,  $z = 25$  nm,  $\varepsilon = 3$ . The laser intensity was taken  $5 \cdot 10^5$  W/m<sup>2</sup>, and the dimensionless damping factor  $\gamma = 0.015$  (see Appendix D for the details of the simulation method).

is enabled. We have plotted (see Fig. 6) the spectral dependence of stiffness parameter  $\kappa_x$  calculated at the first equilibrium point, labeled by point 1 in Fig. 3 (a). To avoid the dependence of stiffness on the illumination intensity, we have normalized it to the magnitude  $\kappa_0 = F_0/R$ , which is the stiffness of a system where the vacuum pressure force  $F_0$  can be restored when nanoparticle is displaced for one radius from its equilibrium position. One can see that the stiffness has a strong resonant behaviour, which corresponds to the excitation of SPP modes at wavelengths longer than 350 nm. With the increase of the distance from nanoparticle center to the surface the stiffness rapidly drops, as the coupling with the SPP mode decreases.

From Fig. 6 one can see that the spectral maximum of stiffness depends on the height from the surface. This spectral dependence can be understood better by analyzing the analytical expression Eq. (8). In the case of negligible losses in the substrate, one can get a simple expression for the stiffness at the first stable equilibrium point (see Appendix C for more details):

$$\kappa_x \approx \pi |p_x|^2 \frac{(k_{SPP})^3 |k_{1z}|^2 |k_{2z}|}{k_0^2 (1 - \varepsilon_s)} Y_2(q_1) \exp(-|k_{1z}|z). \quad (9)$$

Here  $Y_2(q)$  is the cylindrical Webber function of the second order, and  $q_1$  is the first positive root of  $Y_1(q_1) = 0$ .

Note that in the regime of SPP excitation without ohmic losses the SPP wavevector can be in a range from  $k_0$  to  $+\infty$  when  $1+\varepsilon_s \rightarrow 0$ . With that the expression Eq. (C12) goes to zero in both limiting cases:

$$\kappa_x \xrightarrow[k_{SPP} \rightarrow 0, \infty]{} 0,$$

which implies that the stiffness reaches its maximum at some particular wavelength. This wavelength can be defined for each given distance over substrate  $z$ . The maximal stiffness can be achieved close to SPP resonance when SPP wavevector equals to  $\tilde{k} \approx 6/z \gg k_0$ . Then, the maximal stiffness at the  $n$ -th equilibrium position decreases with distance to substrate as  $z^{-6}$  (see Eq. (C13)):

$$\kappa_{x,n} \sim |p_x|^2 \left(\frac{1}{z}\right)^6 \frac{1}{k_0^2} Y_2(q_{2n+1}). \quad (10)$$

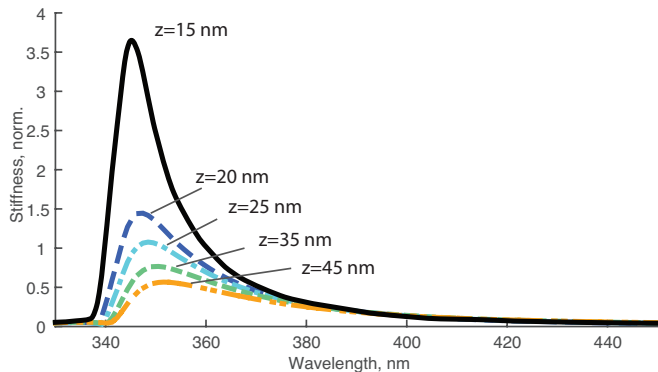


FIG. 6. The stiffness  $\kappa_x$  in units of  $\kappa_0 = F_0/R$  as a function of the excitation wavelength. The spectra are shown for different distances  $z$  from the nanoparticle center to the surface. Nanoparticle radius  $R = 15$  nm.

### III. CONCLUSION

In this work we consider transverse optical binding based on surface plasmon polariton interference. We show that two nanoparticles placed in the vicinity of a plasmonic interface can form a stable bound dimer with binding length defined by the SPP wavelength. This allows formation of the dimers with interparticle distance significantly shorter than the free-space wavelength suppressing the diffractive limit. The binding states are formed along the direction of the incident field polarization, which on the contrary to the photon binding, where the stable bound states are formed perpendicular to the polarization direction. The excitation of SPP modes also enhances the amplitude of the binding forces, resulting in resonant enhancement of the trap stiffness.

#### Appendix A: Calculation of a binding force

The force  $\mathbf{F}_2(\mathbf{r}_2)$  acting on the second nanoparticle is calculated as

$$\mathbf{F}_2(\mathbf{r}_2) = \frac{1}{2} \text{Re} \left[ \sum p_{2i}^*(\mathbf{r}_2) \nabla E_i(\mathbf{r}_2) \right]. \quad (A1)$$

The introduction of the effective polarizability parameters significantly simplifies the formula for the electric field in the center of the second nanoparticle  $\mathbf{E}_2$ :

$$\mathbf{E}(\mathbf{r}_2) = \mathbf{E}_0(\mathbf{r}_2) + \frac{k_0^2}{\varepsilon_0} \hat{G}_s(\mathbf{r}_2, \mathbf{r}_2) \mathbf{p}_2 + \frac{k_0^2}{\varepsilon_0} \hat{G}(\mathbf{r}_2, \mathbf{r}_1) \mathbf{p}_1. \quad (A2)$$

The dipole moments then can be expressed as:

$$\mathbf{p}_1 = \hat{\alpha}_{1,eff}^s \mathbf{E}(\mathbf{r}_1) = \hat{\alpha}_{1,eff}^s \left( \mathbf{E}_0(\mathbf{r}_1) + \frac{k_0^2}{\varepsilon_0} \hat{G}(\mathbf{r}_1, \mathbf{r}_2) \mathbf{p}_2 \right), \quad (A3)$$

$$\mathbf{p}_2 = \hat{\alpha}_{2,eff}^s \left( \mathbf{E}_0(\mathbf{r}_2) + \frac{k_0^2}{\varepsilon_0} \hat{G}(\mathbf{r}_2, \mathbf{r}_1) \mathbf{p}_1 \right), \quad (A4)$$

$$\hat{\alpha}_{i,eff}^s(\mathbf{r}_i, \omega) = \alpha(\omega) \left( 1 - \alpha(\omega) \frac{k_0^2}{\varepsilon_0} \hat{G}_s(\mathbf{r}_i, \mathbf{r}_i, \omega) \right)^{-1}, \quad (A5)$$

$$i = 1, 2.$$

Let us solve this equation system. After some manipulations one can get

$$\mathbf{p}_1 = \hat{\alpha}_{1,eff}^s \left( \mathbf{E}_0(\mathbf{r}_1) + \frac{k_0^2}{\varepsilon_0} \hat{G}(\mathbf{r}_1, \mathbf{r}_2) \left( \hat{\alpha}_{2,eff}^s \left[ \mathbf{E}_0(\mathbf{r}_2) + \frac{k_0^2}{\varepsilon_0} \hat{G}(\mathbf{r}_2, \mathbf{r}_1) \mathbf{p}_1 \right] \right) \right), \quad (A6)$$

$$\mathbf{p}_1 = \hat{\alpha}_{1,eff}^s \left( \mathbf{E}_0(\mathbf{r}_1) + \frac{k_0^2}{\varepsilon_0} \hat{G}(\mathbf{r}_1, \mathbf{r}_2) \hat{\alpha}_{2,eff}^s \mathbf{E}_0(\mathbf{r}_2) \right) + \frac{k_0^4}{\varepsilon_0^2} \hat{\alpha}_{1,eff}^s \hat{G}(\mathbf{r}_1, \mathbf{r}_2) \hat{\alpha}_{2,eff}^s \hat{G}(\mathbf{r}_2, \mathbf{r}_1) \mathbf{p}_1, \quad (A7)$$

The last expression in (A6) can be simplified even fur-

ther, if one renormalizes the effective polarizability tensor with account for nanoparticle cross action:



$$\widehat{\alpha}_{i,eff}^r(\mathbf{r}_i, \omega) = \alpha_i(\omega) \left( 1 - \alpha_i(\omega) \frac{k^2}{\varepsilon_0} \widehat{G}_s(\mathbf{r}_i, \mathbf{r}_i, \omega) - \frac{k^4}{\varepsilon_0^2} \alpha_i \widehat{G}(\mathbf{r}_i, \mathbf{r}_j) \widehat{\alpha}_{j,eff}^s \widehat{G}(\mathbf{r}_j, \mathbf{r}_i) \right)^{-1}, \quad i = 1, 2 \quad j = 2, 1. \quad (\text{A8})$$

Here the self-action Green's function  $\widehat{G}_s(\mathbf{r}_i, \mathbf{r}_i)$  contains the scattered part only, whereas the cross-action part  $\widehat{G}(\mathbf{r}_i, \mathbf{r}_j) = \widehat{G}_0(\mathbf{r}_i, \mathbf{r}_j) + \widehat{G}_s(\mathbf{r}_i, \mathbf{r}_j)$  include both vacuum and scattered parts determining the cross-interaction through vacuum and via substrate respectively. The final expression for the dipole moment will be as follows:

$$\mathbf{p}_i = \widehat{\alpha}_{i,eff}^r \left( \mathbf{E}_0(\mathbf{r}_i) + \frac{k^2}{\varepsilon_0} \widehat{G}(\mathbf{r}_i, \mathbf{r}_j) \widehat{\alpha}_{j,eff}^s \mathbf{E}_0(\mathbf{r}_j) \right), \quad (\text{A9})$$

$$i = 1, 2 \quad j = 2, 1 \quad (\text{A10})$$

The case of normal plane wave incidence on a planar substrate, when the nanoparticles are located at the same height above the surface (see Fig.1) is of a particular interest. In this case the external electric field  $\mathbf{E}_0$  is equal in the centres of both nanoparticles, and, thus, the dipole moment has very simple form:

$$\mathbf{p}_i = \widehat{\alpha}_{i,eff}^R \mathbf{E}_0(\mathbf{r}_i), \quad (\text{A11})$$

$$\widehat{\alpha}_{i,eff}^R = \widehat{\alpha}_{i,eff}^r \left( 1 + \frac{k^2}{\varepsilon_0} \widehat{G}(\mathbf{r}_i, \mathbf{r}_j) \widehat{\alpha}_{j,eff}^s \right), \quad (\text{A12})$$

$$i = 1, 2 \quad j = 2, 1.$$

The optical force component, then, can be calculated as

$$F_{2x}(\mathbf{r}_2) = \frac{1}{2} \text{Re} \left[ \sum_{n=x,y,z} p_{2n}^*(\mathbf{r}_2) \partial_{x_2} E_n(\mathbf{r}_2) \right] = \frac{1}{2} \text{Re} \left[ \sum_{n=x,y,z} p_{2n}^*(\mathbf{r}_2) \left( \partial_{x_2} E_{0n}(\mathbf{r}_2) + \frac{k_0^2}{\varepsilon_0} \sum_{m=x,y,z} \partial_{x_2'} G_{s,nm}(\mathbf{r}_2', \mathbf{r}_2) p_{2m} + \frac{k_0^2}{\varepsilon_0} \sum_{m=x,y,z} \partial_{x_2} G_{nm}(\mathbf{r}_2, \mathbf{r}_1) p_{1m} \right) \right]. \quad (\text{A13})$$

The  $y$  and  $z$  components can be calculated with the same expression (A13) by substituting the partial derivative with  $\partial_y$  and  $\partial_z$  correspondingly.

## Appendix B: Green's function

The Green's function tensor of a two half-spaces with permittivities  $\varepsilon_1$  (for  $z > 0$ ) and  $\varepsilon_2$  (for  $z \leq 0$ ) can be expressed in the cylindrical coordinates through the reciprocal representation in wave-vector space<sup>35</sup> (for  $z > 0$ ):

$$\widehat{G}(\rho, \varphi, z > 0) = \frac{ik_1}{8\pi} \int_0^\infty \widehat{M}(s, \rho, \varphi) \exp(is_{z1}z) ds, \quad (\text{B1})$$

where  $k_1$  is the wavevector in the upper space, and  $s = k_r/k_0$  and  $s_{z1} = k_{z1}/k_0$  are the radial and  $z$ -components of the dimensionless wavevector normalized over the wavevector in the free space.

$$\widehat{M}(s, \rho, \varphi) = \begin{pmatrix} m_{xx} & m_{xy} & m_{xz} \\ m_{yx} & m_{yy} & m_{yz} \\ m_{zx} & m_{zy} & m_{zz} \end{pmatrix} \quad (\text{B2})$$

$$m_{xx} = \frac{s}{s_{z1}} r_s f(s, \rho, \varphi) - s s_{z1} r_p g(s, \rho, \varphi),$$

$$m_{yy} = \frac{s}{s_{z1}} r_s g(s, \rho, \varphi) - s s_{z1} r_p f(s, \rho, \varphi),$$

$$m_{zz} = 2\pi J_0(s\rho) r_p \frac{s^3}{s_{z1}},$$

$$m_{xy} = m_{yx} = \frac{(r_s + s_{z1}^2 r_p)}{s s_{z1}} h(s, \rho, \varphi),$$

$$m_{xz} = -m_{zx} = -s r_p t(s, \rho, \varphi),$$

$$m_{yz} = -m_{zy} = -s r_p w(s, \rho, \varphi),$$

where the functions  $f(s, \rho, \varphi)$ ,  $g(s, \rho, \varphi)$ ,  $h(s, \rho, \varphi)$ ,  $t(s, \rho, \varphi)$ ,  $w(s, \rho, \varphi)$  can be expressed:

$$f(s, \rho, \varphi) = 2\pi \left( \sin^2(\varphi) J_0(s\rho) + \frac{J_1(s\rho)}{s\rho} \cos(2\varphi) \right),$$

$$g(s, \rho, \varphi) = 2\pi \left( \cos^2(\varphi) J_0(s\rho) - \frac{J_1(s\rho)}{s\rho} \cos(2\varphi) \right),$$

$$h(s, \rho, \varphi) = \pi s^2 J_2(s\rho) \sin(2\varphi), \quad (\text{B3})$$

$$t(s, \rho, \varphi) = 2\pi i s J_1(s\rho) \cos(\varphi),$$

$$w(s, \rho, \varphi) = 2\pi i s J_1(s\rho) \sin(\varphi).$$

Here  $J_n(z)$  is the first kind Bessel function of the order  $n$ .

## Appendix C: Analytical expression

Here we analyze the  $x$ -component of the optical force acting on nanoparticles when normal incident light is polarized along the  $x$ -axis. This is the case considered in Fig. 3. According to Eq.(1) the expression for the force will be as follows:

$$F_x = \frac{1}{2} \text{Re} \left( \sum_i p_i(\mathbf{r})^* \partial_x E_i(\mathbf{r}_i) \right). \quad (\text{C1})$$

In order to get a simple analytical result showing all the key features of the SPP-assisted force, we will take into account that the effective  $\hat{\alpha}^R$  tensor has diagonal domination, which implies that  $\alpha_{ii}^R \gg \alpha_{ij}^R$ ,  $i \neq j$ .

The the expression (C1) can be simplified:

$$F_x = \frac{1}{2} \text{Re}(p_x^* \partial_x E_x^s). \quad (\text{C2})$$

The electrical field generated by the dipole at the distance  $\mathbf{r}$  from the first nanoparticle can be expressed through the Green's function  $E_x^s(\mathbf{r}) = 4\pi k_0^2 G_{s,xx}(\mathbf{r}, 0) p_x$ .

Then we have an expression for the lateral component of the optical force written in a very simple form:

$$F_x = 2\pi k_0^2 |p_x|^2 \text{Re}(\partial_x G_{s,xx}(\mathbf{r}, 0)) \quad (\text{C3})$$

The Greens function is expressed through the integral

$$\begin{aligned} G_{s,xx}(x, y, z) &= G_{s,xx}(\rho, \phi, z) = \frac{ik_1}{8\pi^2} \times \quad (\text{C4}) \\ &\int_0^\infty m_{xx}(\rho, s) \exp(is_{1z}z) ds, \\ m_{xx} &= sr_s(s) \frac{a_1(\rho, \phi)}{s_{1z}} - ss_{1z} r_p(s) a_2(\rho, \phi), \\ a_1 &= 2\pi \left( \sin(\phi_0)^2 J_0(s\rho) + \frac{J_1(s\rho)}{s\rho} \cos(2\phi_0) \right), \\ a_2 &= 2\pi \left( \cos(\phi_0)^2 J_0(s\rho) - \frac{J_1(s\rho)}{s\rho} \cos(2\phi_0) \right), \\ s_{1z} &= \sqrt{1-s^2} \quad s_{2z} = \sqrt{\varepsilon_2-s^2}. \end{aligned}$$

Here we use the same notation as in Appendix B. We are interested only in the component containing  $r_p$  term as only it gives rise to SPP response, and also we put  $\phi = 0$ . Then,

$$\begin{aligned} G_{s,xx}(\rho, \phi, z) &= \frac{ik_1}{8\pi^2} \int_0^\infty m'_{xx}(\rho, s) \exp(is_{1z}z) ds, \quad (\text{C5}) \\ m'_{xx} &= -ss_{1z} r_p(s) a_2(s, \rho), \\ a_2 &= 2\pi \left( J_0(s\rho) - \frac{J_1(s\rho)}{s\rho} \right). \end{aligned}$$

Next, we have

$$\begin{aligned} G_{s,xx}(\rho, \phi, z) &= -\frac{ik_1}{4\pi} \times \\ &\int_0^\infty ss_{1z} r_p(s) \left( J_0(s\rho) - \frac{J_1(s\rho)}{s\rho} \right) \exp(is_{1z}z) ds. \quad (\text{C6}) \end{aligned}$$

With this we need to compute  $\partial_x G_{s,xx}$ :

$$\partial_x J_0(s\rho) = k_0 \partial_\rho J_0(s\rho) = -k_0 s J_1(s\rho)$$

$$\partial_x \frac{J_1(s\rho)}{s\rho} = k_0 s \partial_{s\rho} \frac{J_1(s\rho)}{s\rho} = -k_0 s \frac{J_2(s\rho)}{(s\rho)}$$

which gives us

$$\partial_x G_{s,xx}(\rho, 0, z) = \frac{ik_1}{4\pi} k_0 \int_0^\infty s^2 s_{1z} r_p(s) \times \quad (\text{C7})$$

$$\left( J_1(s\rho) - \frac{J_2(s\rho)}{(s\rho)^2} \right) \exp(is_{1z}z) ds. \quad (\text{C8})$$

In order to compute the integral with help of complex analysis, we first continue the integral bounds to  $-\infty, +\infty$  using of the identity:

$$J_n(q) = \frac{1}{2} (H_n^{(1)}(q) - (-1)^n H_n^{(1)}(-q)).$$

$$\begin{aligned} \partial_x G_{s,xx}(\rho, 0, z) &= \frac{ik_1}{8\pi} k_0 \times \\ &\underbrace{\int_{-\infty}^\infty s^2 s_{1z} r_p(s) \left( H_1^{(1)}(s\rho) - \frac{H_2^{(1)}(s\rho)}{(s\rho)} \right) \exp(is_{1z}z) ds}_{I(s)}. \quad (\text{C9}) \end{aligned}$$

Now, using Cauchy theorem we finally evaluate this integral:

$$\begin{aligned} \partial_x G_{s,xx}(\rho, 0, z) &= \frac{ik_1}{8\pi} k_0 2\pi i \text{Res}(I(s))|_{s=\tilde{s}} = \\ &-\frac{k_1}{4} k_0 (\tilde{s})^2 \tilde{s}_{1z} \left( H_1^{(1)}(\tilde{s}\rho) - \frac{H_2^{(1)}(\tilde{s}\rho)}{(\tilde{s}\rho)} \right) \times \quad (\text{C10}) \\ &\exp(i\tilde{s}_{1z}z) \text{Res}(r_p(s))|_{s=\tilde{s}}, \end{aligned}$$

where  $\tilde{s} = \sqrt{\varepsilon_2 \varepsilon_1 / (\varepsilon_1 + \varepsilon_2)}$  is dimensionless wavevector of SPP mode.

Finally, computing the explicit expression for the residue and substituting the obtained results into Eq.(C3) one can get:

$$F_x = \pi |p_x|^2 \text{Re} \left[ \frac{(\tilde{k})^3 (\tilde{k}_{1z})^2 \tilde{k}_{2z}}{k_0^2 (\varepsilon_1 - \varepsilon_2)} \left( H_1^{(1)}(\tilde{k}x) - \frac{H_2^{(1)}(\tilde{k}x)}{(\tilde{k}x)^2} \right) \exp(i\tilde{k}_{1z}z) \right].$$

Here we use dimension variables denoting  $\tilde{k} = \tilde{s}k_0$ , and  $\tilde{k}_{z1,z2} = \tilde{s}_{z1,z2}k_0$ . We can go even further taking into account that  $|H_1^{(1)}(\tilde{k}x)| \ll |J_2(\tilde{k}x)/(\tilde{k}x)^2|$ :

$$F_x \approx \pi |p_x|^2 \text{Re} \left[ \frac{(\tilde{k})^3 (\tilde{k}_{1z})^2 \tilde{k}_{2z}}{k_0^2 (\varepsilon_1 - \varepsilon_2)} H_1^{(1)}(\tilde{k}x) \exp(i\tilde{k}_{1z}z) \right]. \quad (\text{C11})$$

The case of low losses is of special interest. Then, the final expression for the force can be reduced to:

$$F_x = \pi |p_x|^2 \frac{(k^*)^3 |k_{1z}^*|^2 |k_{2z}^*|}{k_0^2 (\varepsilon_1 - \varepsilon_2)} Y_1(k^*r) \exp(-k_{1z}^*z),$$



where  $Y_1(q)$  is the cylindrical Webber function. By expanding this expression around the zeros  $q_n$  of the Webber function  $Y_1(q) \approx -Y_2(q_n)(q - q_n)$ , one can find the expression for the stiffness at the  $n$ -th equilibrium position along  $x$ -axis of the system (see Fig. 3 a):

$$\kappa_n \approx \pi |p_x|^2 \frac{(\tilde{k})^3 |\tilde{k}_{1z}|^2 |\tilde{k}_{2z}|}{k_0^2 (\varepsilon_1 - \varepsilon_2)} Y_2(q_{2n-1}) \exp(-|\tilde{k}_{1z}|z). \quad (\text{C12})$$

Note that in the regime of SPP excitation without ohmic losses the SPP wavevector can be in the range from  $k_0$  to  $+\infty$  when  $\varepsilon_1 + \varepsilon_2 \rightarrow 0$ . With that the expression Eq. (C12) goes to zero in both limiting cases:

$$\kappa_n \xrightarrow{\tilde{k} \rightarrow 0, \infty} 0,$$

which implies that the stiffness reaches its maximum at some particular wavelength. This wavelength can be defined for each given distance over substrate  $z$ . The maximal stiffness can be achieved close to SPP resonance when SPP wavevector equals to  $\tilde{k} \approx 6/z$ . Close to the frequency of SPP resonance when  $\tilde{k} \rightarrow \infty$ , the SPP becomes highly localized close to the interface  $|\tilde{k}_z| \gg k_0$ . Then, the maximal stiffness can be expressed as:

$$\kappa_n \sim |p_x|^2 \left(\frac{6}{z}\right)^6 \frac{1}{k_0^2 \varepsilon_1} Y_2(q_{2n+1}) \exp(-6). \quad (\text{C13})$$

#### Appendix D: Dynamics simulation

We write down the equation of the Newton's equation for the second particle

$$m \frac{d^2}{dt^2} \mathbf{r}_2 = \mathbf{F}_2,$$

where  $\mathbf{F}_2$  is given by (A1) and (A2). One can rewrite it as:

$$\begin{aligned} \frac{d^2}{dt^2} \mathbf{r}_2 = \frac{1}{2m} \sum_i \text{Re} \left\{ p_{2i}^* \nabla \left( E_{0i} + \frac{k^2}{\varepsilon_0} \sum_j G_{s,ij}(\mathbf{r}_2, \mathbf{r}_2) p_{2j} + \right. \right. \\ \left. \left. + \frac{k^2}{\varepsilon_0} \sum_j G_{ij}(\mathbf{r}_2, \mathbf{r}_1) p_{1j} \right) \right\}, \quad i, j = x, y, z \end{aligned} \quad (\text{D1})$$

where  $\hat{G} = \hat{G}_0 + \hat{G}_s$ . In order to decrease the numerical error during numerical simulations, we apply the following natural scaling:

$$\begin{aligned} \boldsymbol{\xi} = \frac{\mathbf{r}}{a}, \quad \tau = \frac{t}{T}, \quad \tilde{\mathbf{E}} = \frac{\mathbf{E}}{E_0}, \quad \tilde{\hat{G}} = a\hat{G}, \\ \tilde{\mathbf{k}} = a\mathbf{k}, \quad \tilde{\mathbf{p}} = \frac{\mathbf{p}}{4\pi\varepsilon_0 a^3 E_0}, \quad \tilde{\alpha} = \frac{\alpha}{4\pi\varepsilon_0 a^3}, \\ T = \sqrt{\frac{m}{2\pi\varepsilon_0 a E_0^2}}. \end{aligned} \quad (\text{D2})$$

After such substitutions we have

$$\begin{aligned} \frac{d^2}{d\tau^2} \boldsymbol{\xi}_2 = \sum_i \text{Re} \left\{ \tilde{p}_{2i}^* \frac{\partial}{\partial \boldsymbol{\xi}} \left( \tilde{E}_{0i} + \tilde{k}^2 \sum_j \tilde{G}_{ij}^s(\boldsymbol{\xi}_2, \boldsymbol{\xi}_2) \tilde{p}_{2j} + \right. \right. \\ \left. \left. + \tilde{k}^2 \sum_j \tilde{G}_{ij}(\boldsymbol{\xi}_2, \boldsymbol{\xi}_1) \tilde{p}_{1j} \right) \right\}. \end{aligned} \quad (\text{D3})$$

We also include the viscosity of the environment by adding the damping factor  $\gamma$ :

$$\frac{d^2}{d\tau^2} \boldsymbol{\xi}_2 = \tilde{\mathbf{F}}_2(\boldsymbol{\xi}_1, \boldsymbol{\xi}_2) - \gamma \frac{d}{d\tau} \boldsymbol{\xi}_2, \quad (\text{D4})$$

where  $\tilde{\mathbf{F}}_2$  is given by the r.h.s. of Eq. (D3). Expression (D4) was a target for the numerical simulation. As a good compromise between stability and computational complexity the Runge-Kutta of fourth-order method was applied. Due to the fact that the motion along  $z$  axis is fixed, we have plane symmetry, which simplifies the force function to  $\tilde{\mathbf{F}}_2(\boldsymbol{\xi}_1, \boldsymbol{\xi}_2) = \tilde{\mathbf{F}}_2(\boldsymbol{\xi}_1 - \boldsymbol{\xi}_2)$ .

#### Appendix E: Conservative vs non-conservative force components

Here we present the results of calculation of total optical force and the conservative component only. By excluding imaginary part of polarizability one can isolate the conservative force only<sup>35</sup>. The result are shown in Fig. 7. One can see that for the considered set of parameters the conservative force strongly dominates over non-conservative, which is the the difference between the total and conservative forces.

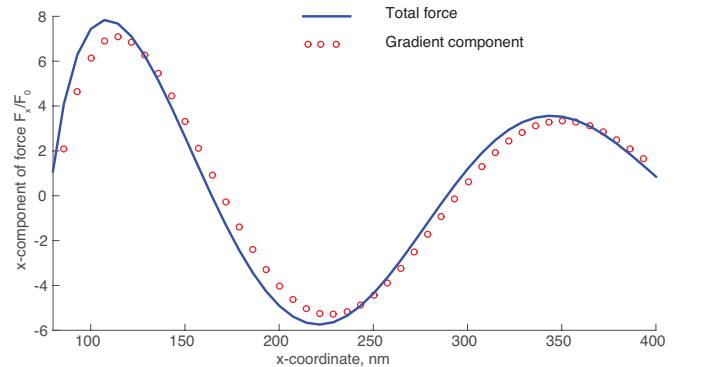


FIG. 7. The total force (blue solid line) and the conservative (red circles) components of the optical force are shown for different wavelengths. The parameters of the calculation are the same as in Fig. 2.

- <sup>1</sup> O. M. Maragò, P. H. Jones, P. G. Gucciardi, G. Volpe, and A. C. Ferrari, *Nature Nanotechnology* **8**, 807 (2013).
- <sup>2</sup> I. Bloch, J. Dalibard, and S. Nascimbène, *Nature Physics* **8**, 267 (2012).
- <sup>3</sup> A. Ashkin, *Physical Review Letters* **24**, 156 (1970).
- <sup>4</sup> V. S. Letokhov, *JETP Letters* **7**, 348 (1968).
- <sup>5</sup> M. M. Burns, J. M. Fournier, and J. A. Golovchenko, *Physical Review Letters* **63**, 1233 (1989).
- <sup>6</sup> M. M. Burns, J. M. Fournier, and J. A. Golovchenko, *Science (New York, N.Y.)* **249**, 749 (1990).
- <sup>7</sup> F. Depasse and J. M. Vigoureux, *Journal of Physics D: Applied Physics* **27**, 914 (1994).
- <sup>8</sup> P. C. Chaumet and M. Nieto-Vesperinas, *Physical Review B* **64**, 035422 (2001), arXiv:0305045 [physics].
- <sup>9</sup> J. Kesava, P. C. Chaumet, T. Langtry, and A. Rahmani, *Journal of Nanophotonics* **4**, 041583 (2010).
- <sup>10</sup> M. Mazilu, A. Rudhall, E. M. Wright, and K. Dholakia, *Journal of Physics: Condensed Matter* **24**, 464117 (2012).
- <sup>11</sup> S. Sukhov, A. Shalin, D. Haefner, and A. Dogariu, *Optics express* **23**, 247 (2015).
- <sup>12</sup> R. W. Bowman and M. J. Padgett, *Reports on progress in physics. Physical Society (Great Britain)* **76**, 026401 (2013).
- <sup>13</sup> M.-T. Wei, J. Ng, C. T. Chan, and H. D. Ou-Yang, *Scientific Reports* **6**, 38883 (2016).
- <sup>14</sup> L. Chvatal, O. Brzobohaty, and P. Zemanek, *Optical Review* **22**, 157 (2015).
- <sup>15</sup> V. Demergis and E. L. Florin, *Nano Letters* **12**, 5756 (2012).
- <sup>16</sup> S. H. Simpson, P. Zemánek, O. M. Maragò, P. H. Jones, and S. Hanna, *Nano Letters* **17**, 3485 (2017).
- <sup>17</sup> M. M. Salary and H. Mosallaei, *Physical Review B - Condensed Matter and Materials Physics* **94**, 1 (2016).
- <sup>18</sup> C. Van Vlack, P. Yao, and S. Hughes, *Physical Review B - Condensed Matter and Materials Physics* **83**, 1 (2011), arXiv:1102.0794.
- <sup>19</sup> M. L. Juan, M. Righini, and R. Quidant, *Nature Photonics* **5**, 349 (2011).
- <sup>20</sup> R. Quidant and C. Girard, *Laser and Photonics Reviews* **2**, 47 (2008).
- <sup>21</sup> A. S. Shalin and S. V. Sukhov, *Plasmonics* **8**, 625 (2013).
- <sup>22</sup> A. S. Shalin, S. V. Sukhov, A. A. Bogdanov, P. A. Belov, and P. Ginzburg, *Physical Review A* **91**, 063830 (2015).
- <sup>23</sup> A. A. Bogdanov, A. S. Shalin, and P. Ginzburg, *Scientific Reports* **5**, 15846 (2015), arXiv:arXiv:1506.01754v1.
- <sup>24</sup> V. Garces-Chavez, R. Quidant, P. J. Reece, G. Badenes, L. Torner, and K. Dholakia, *Physical Review B - Condensed Matter and Materials Physics* **73**, 1 (2006).
- <sup>25</sup> G. Volpe, R. Quidant, G. Badenes, and D. Petrov, *Physical Review Letters* **96**, 1 (2006).
- <sup>26</sup> M. Yuan, L. Cheng, P. Cao, X. Li, X. He, and X. Zhang, *Plasmonics*, 1 (2017).
- <sup>27</sup> Z. Yan, Y. Bao, U. Manna, R. A. Shah, and N. F. Scherer, *Nano Letters* **14**, 2436 (2014).
- <sup>28</sup> C. Min, Z. Shen, J. Shen, Y. Zhang, H. Fang, G. Yuan, L. Du, S. Zhu, T. Lei, and X. Yuan, *Nature communications* **4**, 2891 (2013).
- <sup>29</sup> S. B. Wang and C. T. Chan, *Nature communications* **5**, 3307 (2014).
- <sup>30</sup> M. I. Petrov, S. V. Sukhov, A. A. Bogdanov, A. S. Shalin, and A. Dogariu, *Laser and Photonics Reviews* **10**, 116 (2016), arXiv:1601.01863.
- <sup>31</sup> A. Ivinskaya, M. I. Petrov, A. A. Bogdanov, I. Shishkin, P. Ginzburg, and A. S. Shalin, *Light: Science & Applications* **6**, e16258 (2017).
- <sup>32</sup> F. J. Valdivia-Valero and M. Nieto-Vesperinas, *Optics express* **20**, 13368 (2012).
- <sup>33</sup> J. M. Auñón, F. J. Valdivia-Valero, and M. Nieto-Vesperinas, *Journal of the Optical Society of America. A, Optics, image science, and vision* **31**, 206 (2014).
- <sup>34</sup> P. C. Chaumet and M. Nieto-Vesperinas, *Optics Letters* **25**, 1065 (2003), arXiv:0305043 [physics].
- <sup>35</sup> L. Novotny and B. Hecht, *Principles of Nano-Optics* (Cambridge University Press, 2012) p. 578.
- <sup>36</sup> K. Dholakia and P. Zemánek, *Reviews of Modern Physics* **82**, 1767 (2010).